CHALMERS
UNIVERSITY OF TECHNOLOGY

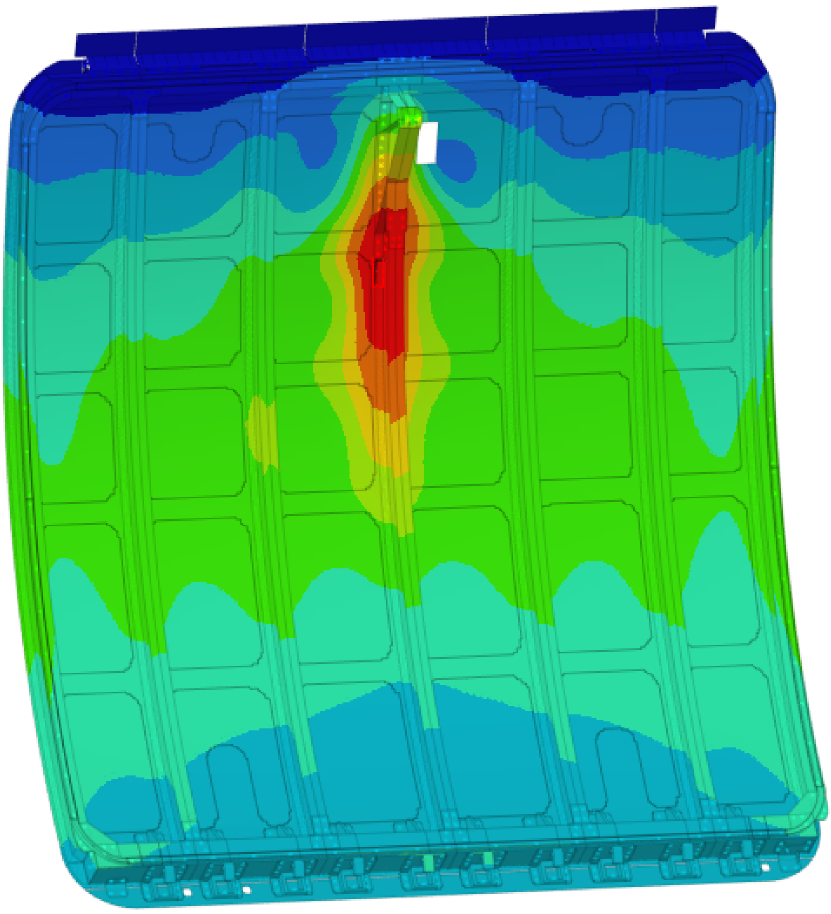

Analysis and test definition of adhesively bonded joints in aircraft structures

PRASHANT ANIL TIWARI

DEPARTMENT OF INDUSTRIAL AND MATERIALS SCIENCE
CHALMERS UNIVERSITY OF TECHNOLOGY
Gothenburg, Sweden 2022
www.chalmers.se

Master's thesis 2022

Analysis and test definition of adhesively bonded joints in aircraft structures

PRASHANT ANIL TIWARI

CHALMERS
UNIVERSITY OF TECHNOLOGY

Department of Industrial and Materials Sciences
Division of Material and Computational Mechanics
Chalmers University of Technology
Gothenburg, Sweden 2022

Analysis and test definition of adhesively bonded joints in aircraft structures

PRASHANT ANIL TIWARI

Supervisor: Tomas Lundgren, SAAB AB
Examiner: Prof. Leif Asp, Department of Industrial and Materials Science

Master's Thesis 2022
Department of Industrial and Materials Science
Division of Material and Computational Science
Chalmers University of Technology
SE-412 96 Gothenburg
Telephone +46 31 772 1000

Cover: Displacement contour plot for critical jam load case in the cargo door.

Typeset in LaTeX
Printed by Chalmers Reproservice
Gothenburg, Sweden 2022

Analysis and test definition of adhesively bonded joints in aircraft structures
Master thesis report
PRASHANT ANIL TIWARI
Department of Industrial and Material Science
Chalmers University of Technology

Abstract

This report covers the analyses of the adhesively bonded joints in the cargo door of the Clean Sky 2 project FMCD. Adhesives undergo large rotation and its failure is dependent on hydrostatic and deviatoric stresses. Extended Drucker-Prager method has been used to capture the elastoplastic response of the adhesive in FEM. Adhesives and adherends are modelled as hexahedral elements. Spew fillets are used to reduce the effect of singularities at the edge of the joints. To keep the computational time less, only the critical location is modelled with solid adhesive and adherends. 1D elements with adhesive material properties are used to model the non critical regions. The FE method shows promising results at the critical regions where analytical method did not.

Keywords: aircraft, adhesive, Finite element method, Drucker-Prager.

List of Acronyms

Below is the list of acronyms that have been used in this report listed in alphanumerical order:

DOF	Degrees of freedom
E	Elastic Modulus
FE	Finite Element
FEM	Finite Element Method
FMCD	Future Metallic Cargo door
HT	Hot Temperature
ITD	Integrated Technology Demonstrator
I_1	First Invariant of Cauchy stress
J_2	Second Invariant of the deviatoric part of Cauchy stress
RT	Room Temperature
SLJ	Single Lap Joint
1D	One dimensional
2D	Two dimensional
3D	Three dimensional

Acknowledgements

I wish to show my appreciation to my superviosr at SAAB AB, Tomas Lundgren, who guided me throughout this porject. I would like to express my gratidue to Sofia Lönnelid Mundel at SAAB AB, for giving me this opportunity. I am also grateful to Prof. Leif Asp at Chalmers University for his guidance and support during this project. Finally, I would like to thank my friends and family who supported me and offered deep insight into the study.

Prashant Anil Tiwari, Gothenburg, June 2022

Contents

List of Figures

List of Tables

1

Introduction

1.1 Background

Clean Sky 2 is a public-private partnership between the European Commission and the European aeronautics industry working to develop innovative technologies to cut aircraft emissions of CO_2 and other greenhouse gases and reduce noise. SAAB has been using bonded joints in aircraft structures since SAAB 340, which was introduced in the commercial market in the "1980s". SAAB in Clean Sky 2 ITD airframe FMCD project manufactured a full-scale cargo door with adhesively bonded joints.

Adhesively bonded joints offer several advantages over traditional joints (welded, riveted, or bolted) such as the absence of damage in the bonded parts, ease of manufacturing, reduced weight, uniform stress distribution, and the possibility of joining dissimilar material. The presence of rubber particles in adhesives makes it elastic and it presents extensive non-linear deformation before rupture. The geometrical features such as joint shape, dimensions, or fillets have a significant influence on stress and strain levels in the critical region. Hence, the analysis method of the adhesively bonded joint must account for the material and geometrical non-linearity.

The finite element method provides a powerful calculation tool for the analysis and design of adhesively bonded joints. It is possible to determine the exact stress-strain distribution in the adhesive for any loading condition. The material model within the FE technique plays an important role to capture the loading response of the adhesive. Drucker-Prager has been extensively used to model the elastoplasic behaviour of adhsesives [1]. García et al. showed a method to extract the material data required for Drucker-prager method [1]. Muhammet et al. shows that including a spew fillet in the FE analysis reduces the singularity stress at the joint corners and edges [2].

1.2 Scope

The scope of the thesis is to get a better understanding of the strength characteristics of adhesively bonded joints. Loads required for static and fatigue strength checks are extracted from the FEM. The most important task of this project is to validate the critical joints in the cargo door. This project also includes determination of best FE modelling techniques and a test plan proposal.

1.3 Boundaries

Conducting the coupon test and validation of the results is out of scope. Saab's analytical method for static and fatigue strength checks will not be explained in detail in this report as they are company confidential. Modelling a damage such as cohesive zone is not included in this project. Residual stresses produced during curing is not accounted in this project. Thermal loads are also not included.

1.4 Problem formulation

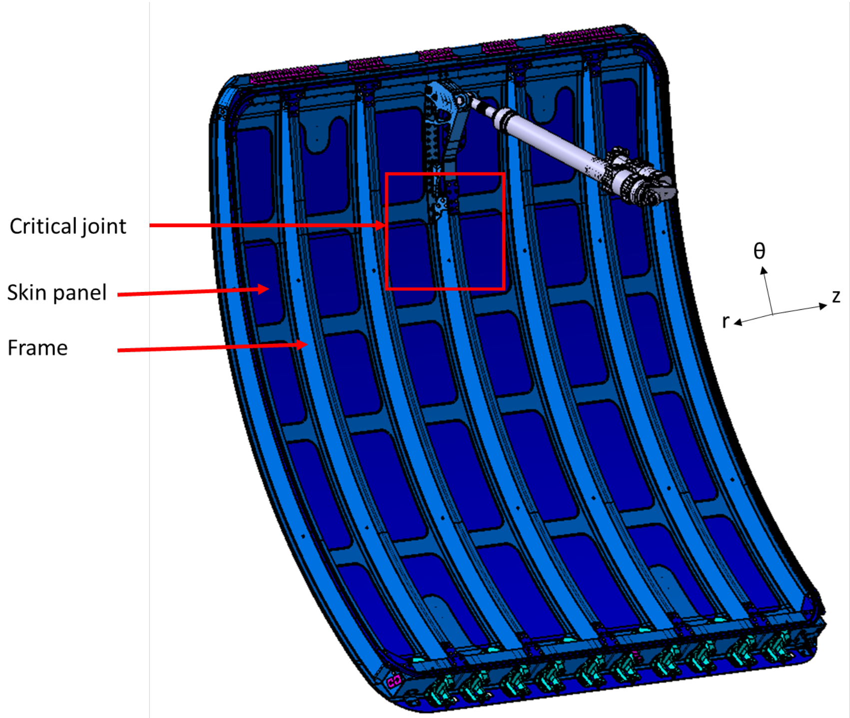

Figure 1.1: Critical joint in the cargo door

Figure 1.1 shows a critical joint in the door along with skin panel and frame. Figure 1.2 depicts typical loads experienced by an adhesively bonded joint. In the nominal FE model, the metallic plates at the critical joint were modelled (discretized) as shell/tetrahedral

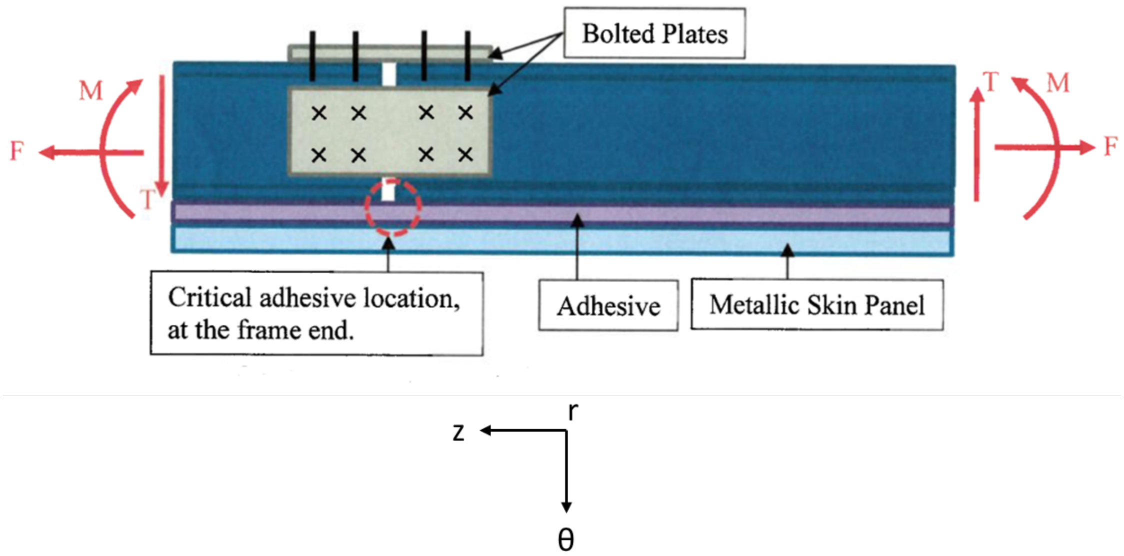

Figure 1.2: Typical design of a bonded skin/frame [3]

elements and the adhesive was by rigid elements (connector elements CONN3D, [4]). Then the strength of the adhesive was calculated by Saab's analytical method.

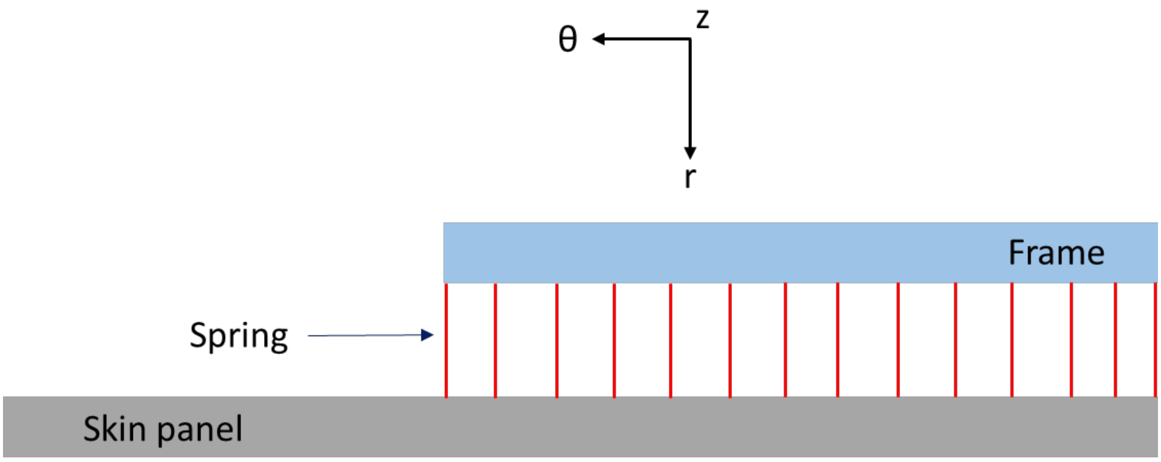

Figure 1.3: Cross sectional view of nominal FE model at the critical joint

A spring element consists of two nodes that are connected to the metallic plates and it has no connection to other spring elements. Hence the load transfer takes place from one metallic plate to another through one spring element and the stress flow within the adhesive film is not captured. The spring elements near the edge of the frame flange shown in Figure 1.3 experience higher stresses compared to their neighbouring elements. To get a better approximation of stresses and the stress flow, the adhesive film will be modelled as either 2D (shell) or 3D (continuum) elements.

1.4.1 Structural Integrity

The cargo door of the Clean Sky 2 project is subjected to static and fatigue loads. The aforementioned joint is subjected to high shear and tensile stresses. The maximum allowable shear and peel stresses are provided which will be used to predict the failure of the joints.

1.4.2 Load cases

Static load cases are ultimate cabin pressurization and door jamming during operation. Fatigue load cases considered are opening and closing sequences of the door and fatigue cabin pressurization.

1.4.3 Material specification

The adhesive used in the Clean Sky 2 ITD airframe FMCD project is AF163-2. The metallic components are made from aluminium alloy. Material data for the adhesive FM73MOST is used in this project as the adhesive AF163-2 is not tested.

2

Theory

2.1 Von Mises Criterion

Von Mises criterion is named after German-American applied mathematician Richard von Mises (1883-1953). According to this criterion, a structural material is safe as long as the maximum distortion energy per unit volume is smaller then the distortion energy per unit volume required to cause yield in a tensile test. This criterion can be expressed as it is shown in equation 2.1.

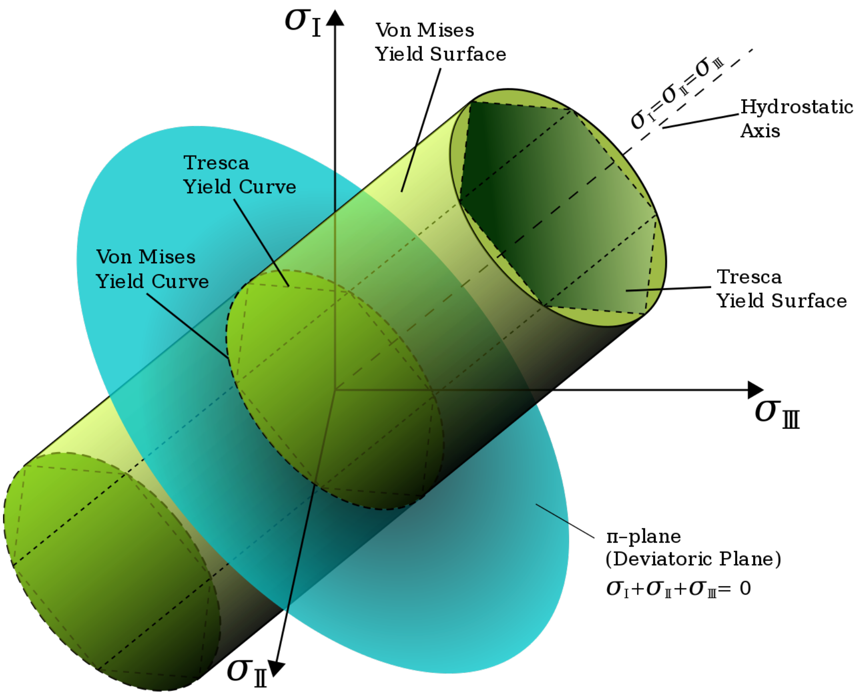

Figure 2.1: Von Mises yield surface [5]

$$\sigma_{yield} = \sqrt{\frac{1}{2}[(\sigma_1 - \sigma_2)^2 + (\sigma_2 - \sigma_3)^2 + (\sigma_3 - \sigma_1)^2]} = \sqrt{3J_2} \tag{2.1}$$

where
σ_i = the principal stresses
σ_{yield} = the tensile/compressive yield stress

J_2 = the second invariant of the deviatoric stress tensor.

As shown in Figure 2.1, this criterion suggests that the yielding initiates as the second invariant of deviatoric stress J_2 reaches a critical value. This criterion suitable for metallic structures is independent of hydrostatic stresses. Plastic model used for metals based on von Mises is also known as J_2 plasticity. Plastic deformation materialises under constant volume condition which implies that tension and compression stresses are same. However, studies have shown that the polymer experiences higher yield stresses in compression than in tension which is a deviation from the classical von Mises yield criterion.

2.2 Drucker-Prager yield criterion

The Drucker-Prager yield criterion is a pressure dependent failure criterion. It was introduced to assess the plastic deformation of soils. The Drucker-Prager yield criterion is given in equation 2.2

$$\sqrt{J_2} = A + BI_1 \tag{2.2}$$

where $I_1 = \Sigma\sigma_i$ is the first invariant of the Cauchy stress and J_2 is the second invariant of the deviatoric part of the Cauchy stress. A and B are material constants.
In terms of the equivalent stress (σ_e) and the hydrostatic stress (σ_m), the Drucker-Prager criterion can be expressed as in equation 2.3

$$\sigma_e = a + b\sigma_m \tag{2.3}$$

Linear Drucker-Prager model offered in Abaqus is used in this project.

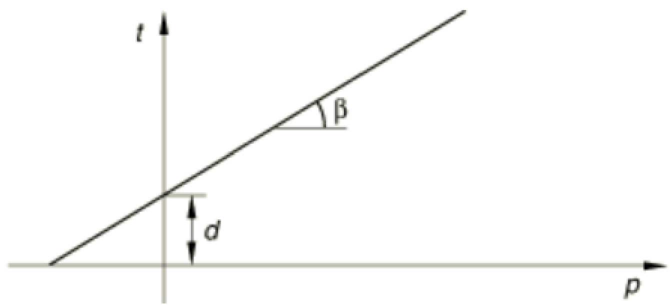

Figure 2.2: Typical yield/Linear Drucker-Prager yielding criterion [4]

The yield criterion shown in Figure 2.2 can be expressed as

$$F = t - ptan\beta - d = 0$$

where

$$t = \frac{1}{2}q\left[1 + \frac{1}{K} - \left(1 - \frac{1}{K}\right)\left(\frac{r}{q}\right)^3\right]$$

β is the slope of the linear yield surface in the p-t stress plane and is generally referred to as the friction angle. K is the ratio of the yield stress in triaxial tension to the yield stress in triaxial compression. The yield surface is shown in Figure 2.3. p is equivalent pressure stress, q is Mises equivalent stress and r is the third invariant of deviatoric stress. d is related to the input data as hardening defined by uniaxial compression, tension or cohesion.

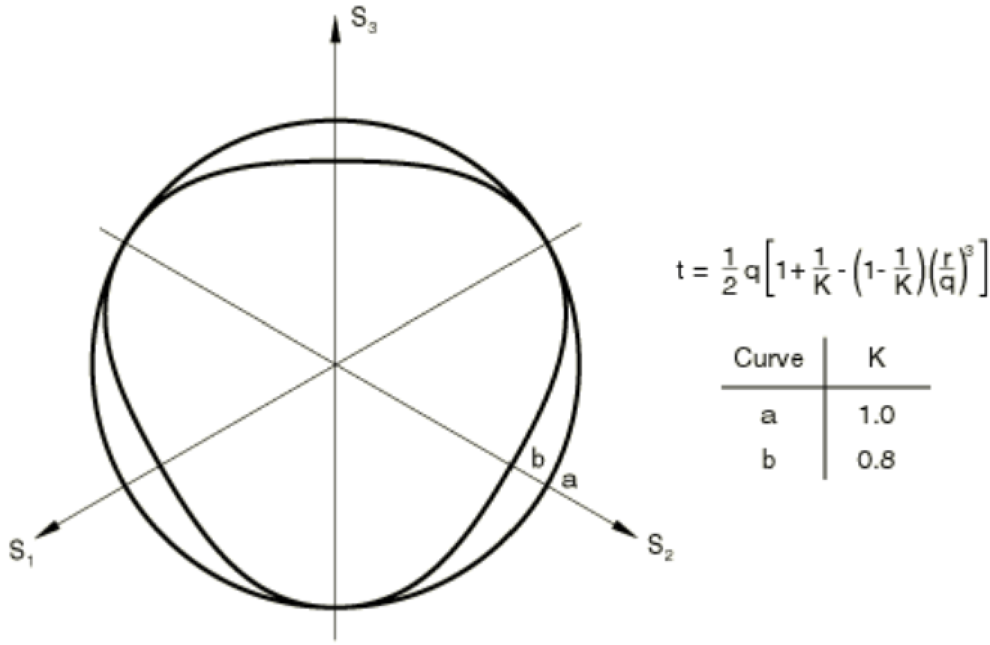

Figure 2.3: Typical yield/flow surfaces of the linear model in the deviatoric plane [4]

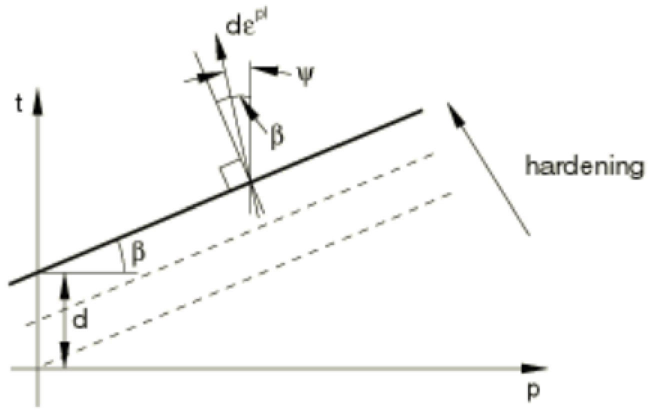

Figure 2.4: Linear Drucker-Prager model: yield surface and flow direction in the t-p plane [4]

The flow potential used in this model is given in equation 2.4

$$G = t - ptan\psi \tag{2.4}$$

where

ψ is the dilation angle in the t-p plane as shown in Figure 2.4. Associated flow is assumed in this project which means dilation angle and friction angle are same, i.e. $\psi = \beta$.

3

Methods

3.1 Local model

The analytical method was designed based on the experimental results. FE models were used to predict the failure of Single Lap Joint (SLJ) in similar loading conditions as of tests. The purpose of the local model is to identify the failure parameters and validate the analytical method.

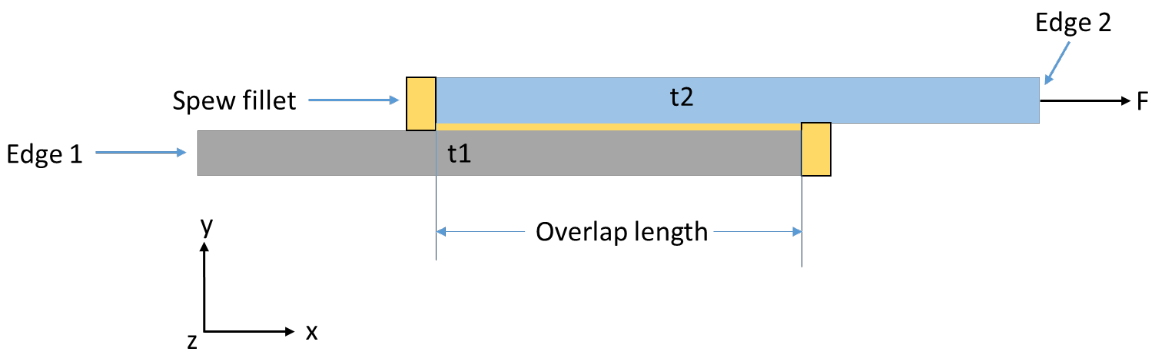

Figure 3.1: Single Lap Joint (SLJ) under influence of tensile load

Figure 3.1 depicts a typical lap joint under a tensile load of magnitude F, which is applied as a distributed load over the edge. t1 and t2 are adherends thicknesses shown in grey and blue colors. Adhesive is shown in yellow. Edge 1 is prevented from translating in x and y direction and rotating around z. Edge 2 is restricted from translating in y-direction.

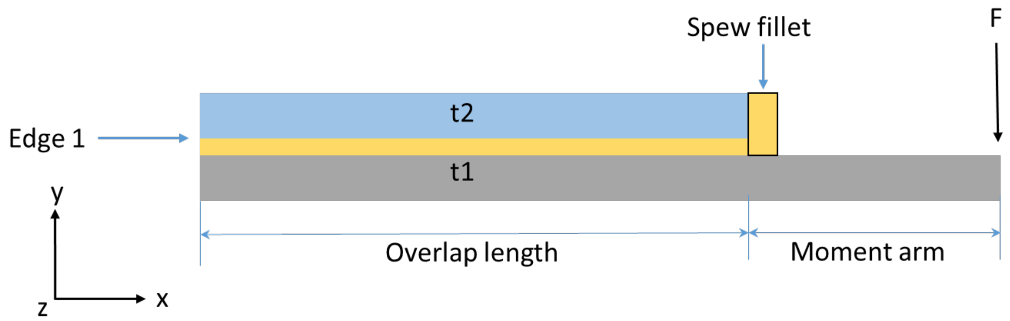

Figure 3.2: Single Lap Joint (SLJ) under influence of transverse load

Figure 3.2 shows a lap joint which is used to predict failure due to the predominating peel stresses. Edge 1 is prevented from translating in x, y and rotating around z-direction. Peel stress produced in this case is influenced by the transverse shear forces and bending moment. The bending load of magnitude F is applied as a point load.

Table 3.1: SLJ dimensions used in the FE models under tensile loads

Joint type	t1 (mm)	t2 (mm)	Overlap length (mm)	Temperature (C)
1	2	2	20	RT
2	2	2	30	RT
3	4	4	20	RT

Table 3.2: SLJ dimensions used in the FE models for transversely loaded condition

Joint Type	t1 (mm)	t2 (mm)	Moment arm (mm)	Temperature (C)	Type
4	2.3	2.5	25	HT	Test
5	2.3	2.5	27	HT	FE
6	2.3	3.2	16	HT	Test
7	2.3	3.2	18	HT	FE
8	2.3	3.2	25	HT	Test
9	2.3	3.2	10.8	HT	FE

The plane strain condition is assumed as the strains in the z-direction will be very small compared to strains in the x and y directions. 2^{nd} order quadratic elements (CPE8 [4]) are used to model both the adherends and adhesive. Adherends and adhesive are connected by using node-to-node connections in all the SLJs. Non-linear geometry with large deformations and Drucker-Prager elastoplastic material models are used in these FE runs. Table 3.1 shows dimensions of SLJ obtained from the test report [6] to be used in the FE models for failure in tensile loading. Table 3.2 shows the specifications of test specimens for failure due to dominating peel stresses. All the items in Table 3.2 have same overlapping length of 40 mm. Both the adherends in Table 3.1 have same length of 75 mm. Data in the Table 3.1 is extracted from [6] and Table 3.2 from [7].

3.2 Global model

The nominal global FE model shown in Figure 3.3, was converted into Abaqus as it was built in Nastran. Abaqus is used in this project to employ numerical techniques such as contact pairs, shell to solid coupling, sub modeling, and plastic material model for adhesives.

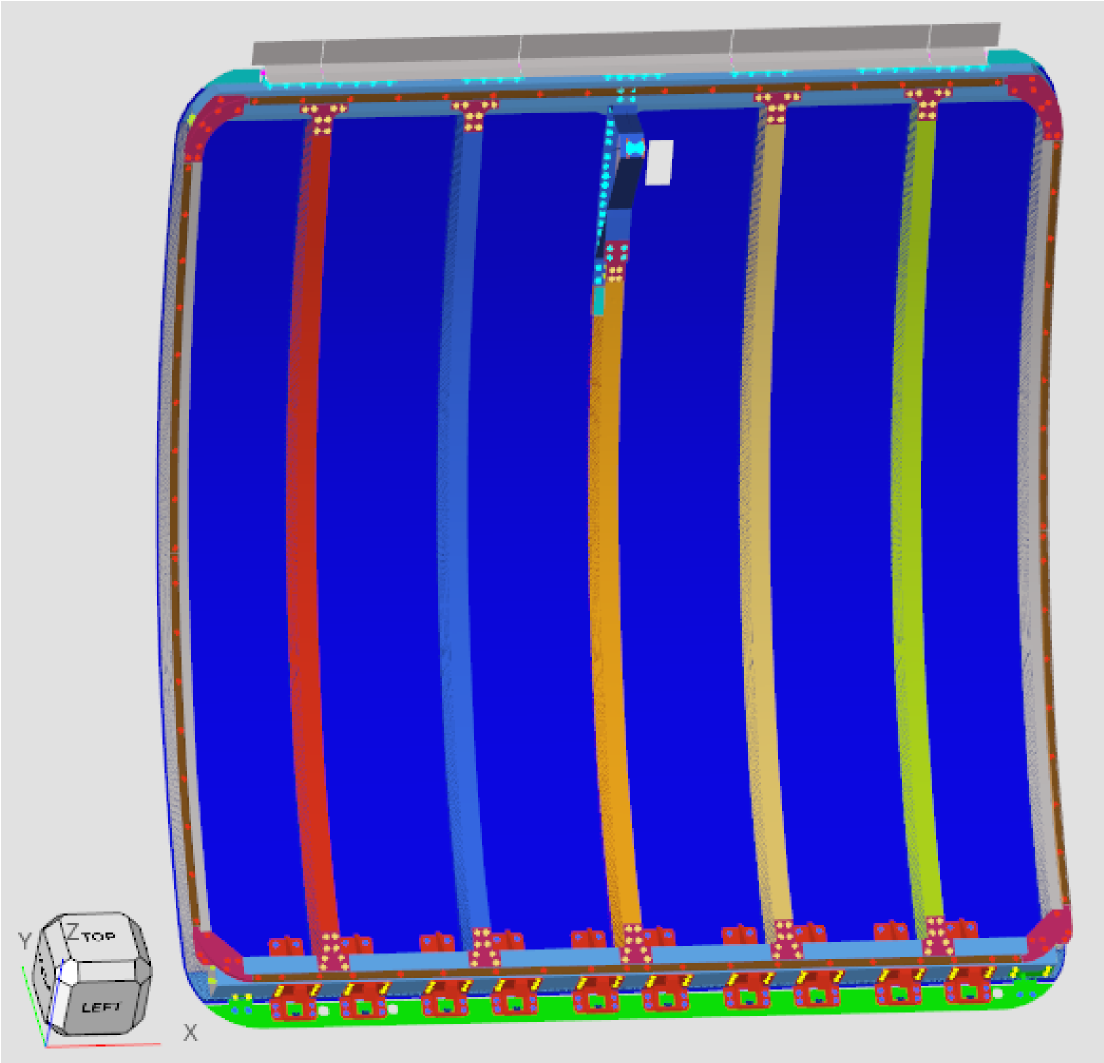

Figure 3.3: Cargo door global finite element model (GFEM)

Adhesives modeled with rigid elements are replaced with 1D beam elements. 1D beam elements (B31 [4]) have 6 active degrees of freedom and stiffness based on elastic modulus of adhesive along with square cross-section area. Figure 3.4 shows the critical location. As the failure prediction is based on all 3 directional stresses, frame lower flange, skin and adhesive are discretized with 3D elements as shown in Figure 3.5. Spew fillet as shown in Figure 3.5 is also included in the model to prevent singularity which are expected at the edges. Shell to solid coupling is used to give connection between shell and solid elements of the same components [4] .

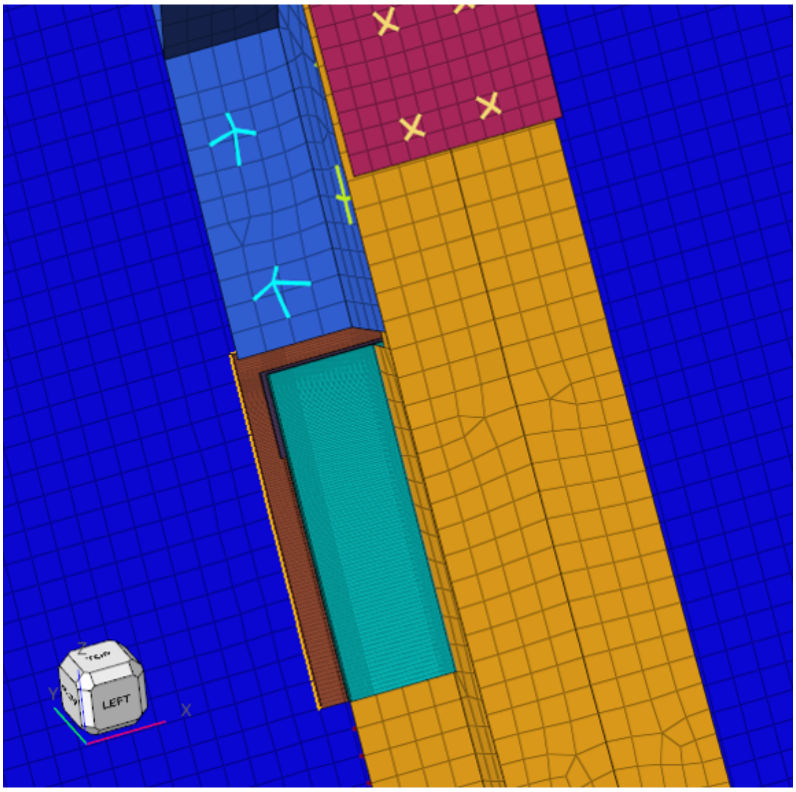

Figure 3.4: Critical location for the failure due to high peel stresses

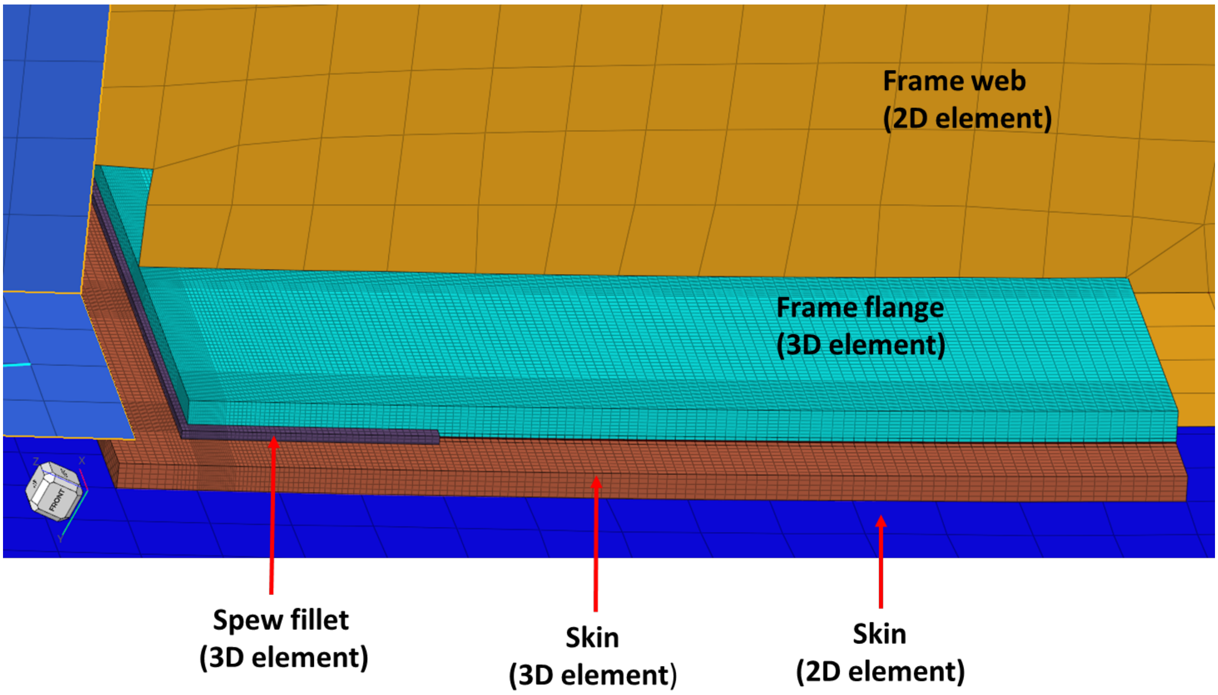

Figure 3.5: Detailed view of critical location of cargo door

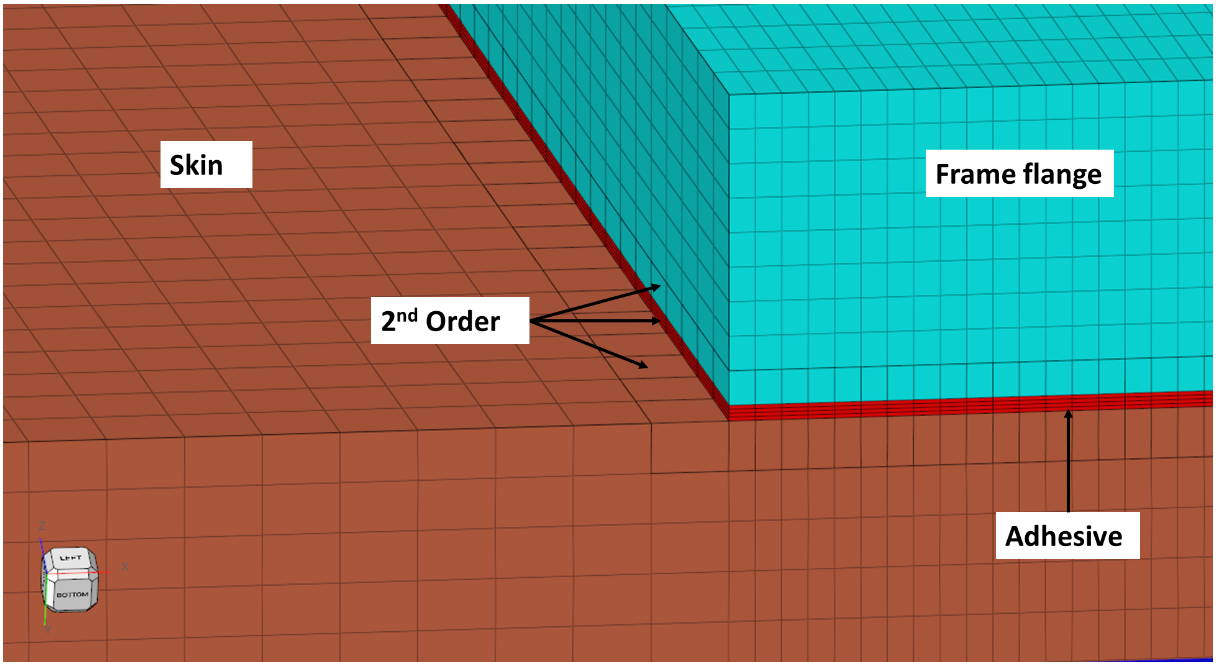

Figure 3.6: Detailed view of critical location depicting element orders used

GFEM includes an adhesive of 0.1 mm in thickness which is small compared to the thickness of skin and frame, as shown in Figure 3.6. The adhesive is discretized with 2^{nd} order hexahedron elements (C3D20R [4]). To reduce the computational time, the elements in adherends adjacent to adhesive are only modelled as 2^{nd} order hexahedral elements and remaining as linear hexahedron elements (C3D8 [4]) as shown in Figure 3.6.

3.3 Load cases

The most critical load case is door jamming during operation which is shown in Figure 3.7. To simulate door jam load case, hinge lugs are prevented from translating in r, θ, and z-directions. Few nodes at the location indicated by BC1 are constrained to prevent motion in radial directions. Actuator load of magnitude F is applied at the lugs of lift fitting mechanism as shown in Figure 3.7.

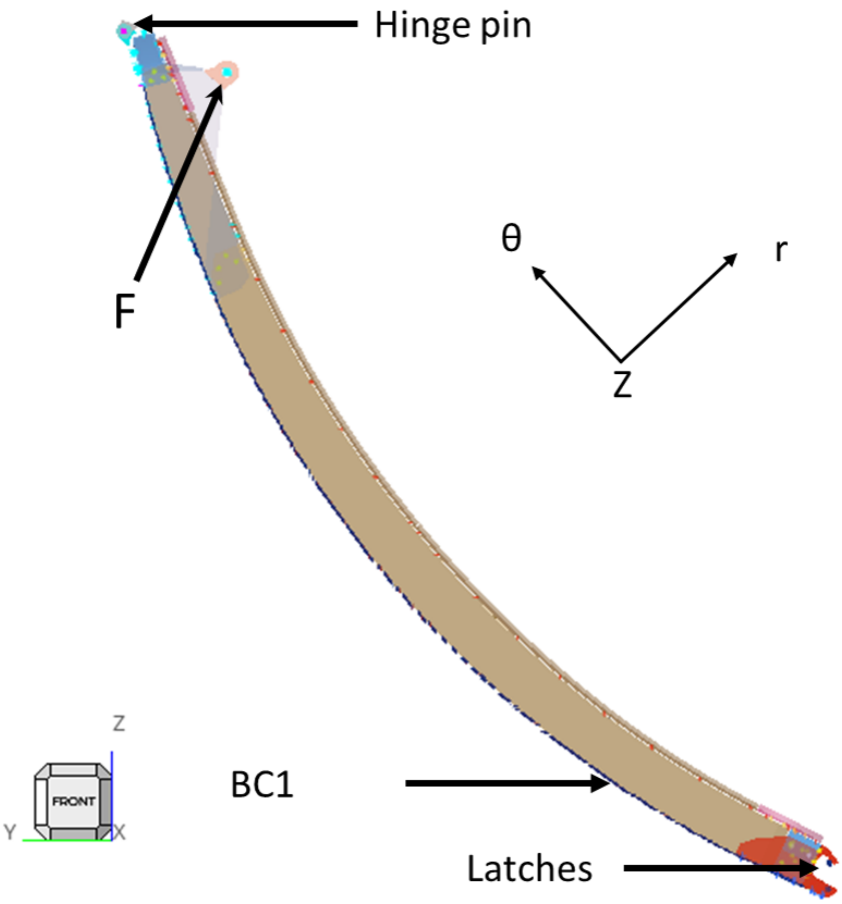

Figure 3.7: Cross sectional view of cargo door with jam load and boundary conditions

Ultimate cabin pressurization is simulated by restricting the nodes at hinge pin and latch lugs are prevented from translating in x, y, and z-directions as shown in Figure 3.8. Pressure is applied on the skin's element faces.

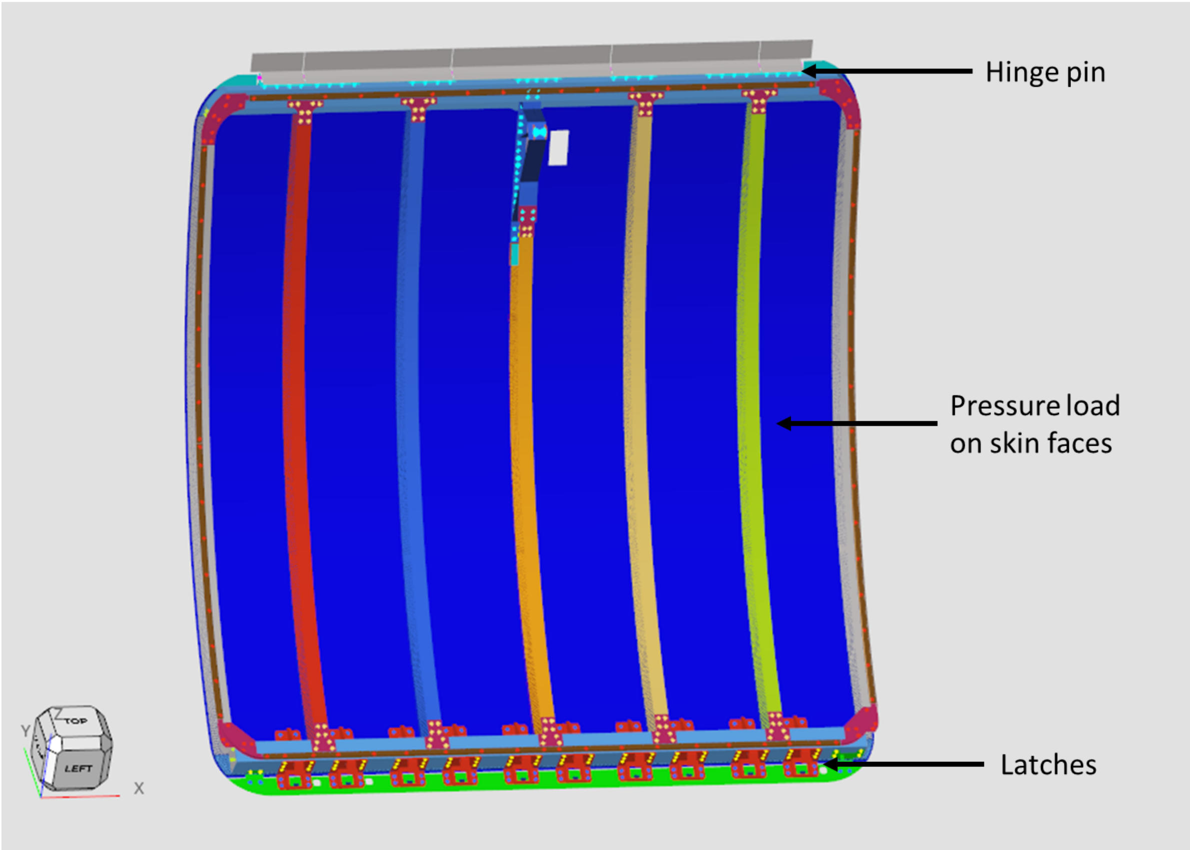

Figure 3.8: Ultimate cabin pressurization load case

3.4 Failure Index

The failure index is a scalar parameter used to quantify the failure phenomena. A failure index of 1 indicates that the equivalent plastic strain obtained from Abaqus is equal to the plastic strain at failure from the test results. The purpose of this index is to avoid the disclosure of allowable. The failure index is expressed in Equation 3.1.

$$\text{Failure Index} = \frac{\text{Equivalent plastic strain}}{\text{Allowable plastic strain or Failure plastic strain}} \tag{3.1}$$

where,
Equivalent plastic strain is obtained from Abaqus (PEEQ, [4]),
Failure plastic strain is obtained from the test results and
Allowable plastic strain is the conservative value of the failure plastic strain.

4

Results

4.1 Local model

4.1.1 Single lap joint under tensile load

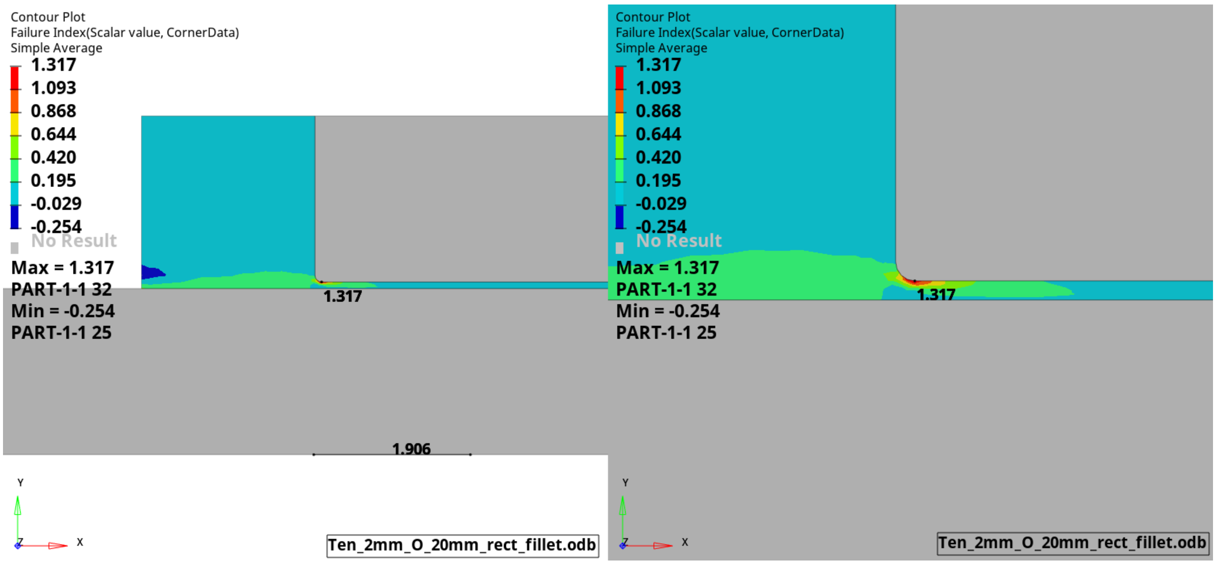

Figure 4.1: Failure index for the SLJ type 1 (left) and its magnified image (right)

Figure 4.1 depicts failure index of SLJ type 1 of Table 3.1. Failure index of 1.317 can be observed in Figure 4.1 which is 0.317 higher but it is localized. Similar behaviour can be observed in Figure 4.2. An index of 1.849 is obtained which is more than the failure plastic strain. However, the region with failure index of 1 and above is small. The hot-spot is observed just below the adherend for type 1 and 2 joints.

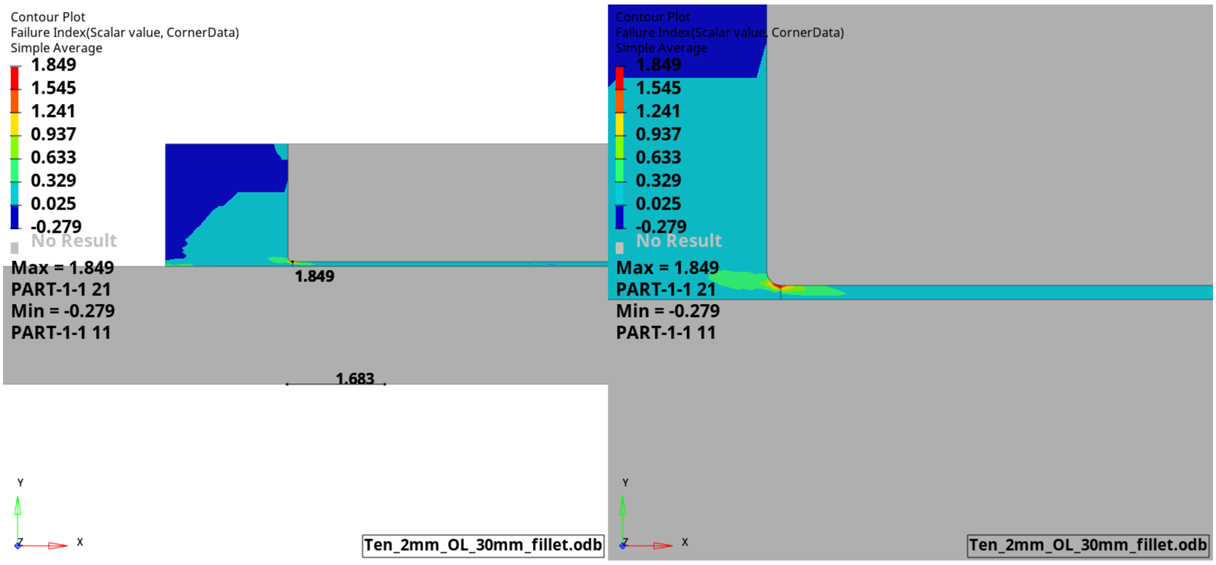

Figure 4.2: Failure index for the SLJ type 2 (left) and its magnified image (right)

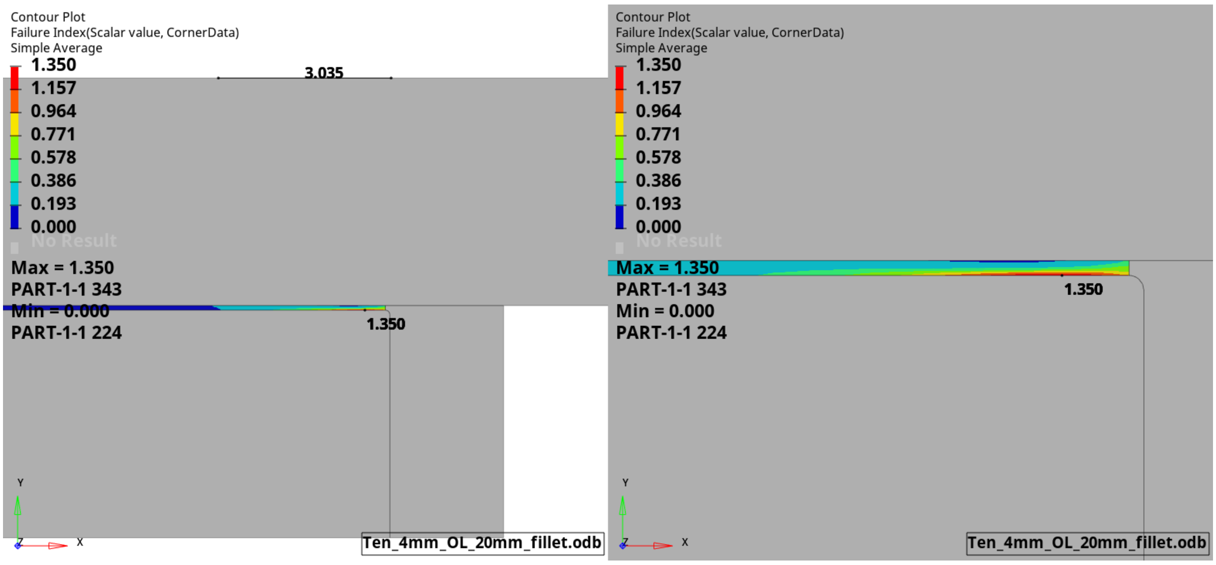

Figure 4.3: Failure index for the SLJ type 3 (left) and its magnified image (right)

The difference between SLJ types 1, 2, and 3 joints as observed in Table 3.1 is that thicker adherends are used in type 3. Figure 4.3 shows the contour plot of the failure index of SLJ type 3. In this type, the region with maximum plastic strain is found to be on the right side as compared to types 2 and 3 in Figures 4.1 and 4.2 respectively, and the hot-spot is obtained at the interface between the adhesive and the adherend.

4.1.2 Transversely loaded single lap joint

4.1.2.1 Experimental tests

Three experimentally tested joints are modelled and results in form of failure index (equivalent plastic strain) is shown in Figures 4.4, 4.5 and 4.6 respectively. SLJs type 4 and 8 show a failure index of 1 while type 6 shows 0.737. The hot-spot is obtained at the interface between adhesive and adherend in all the cases.

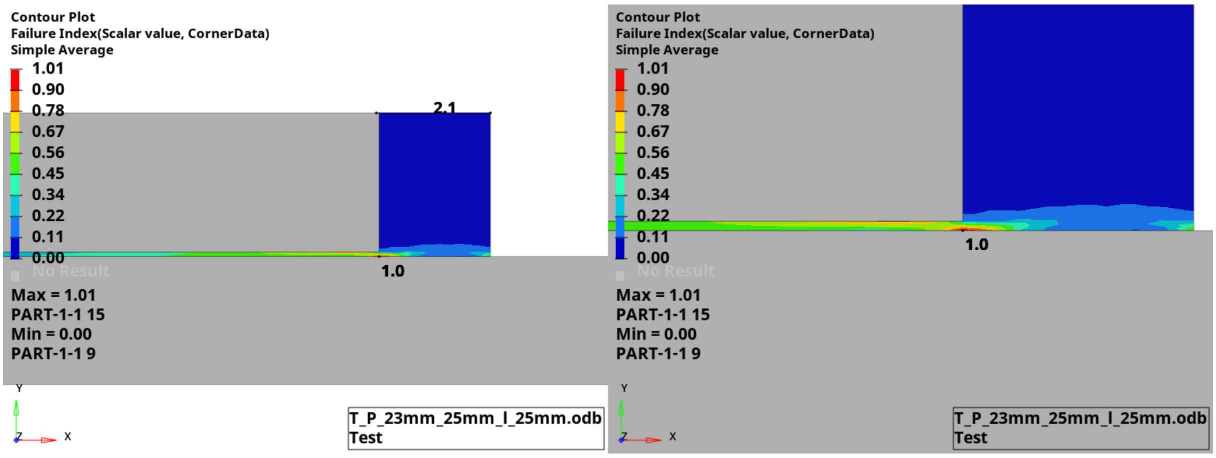

Figure 4.4: Failure index for the SLJ type 4 (left) and its magnified image (right)

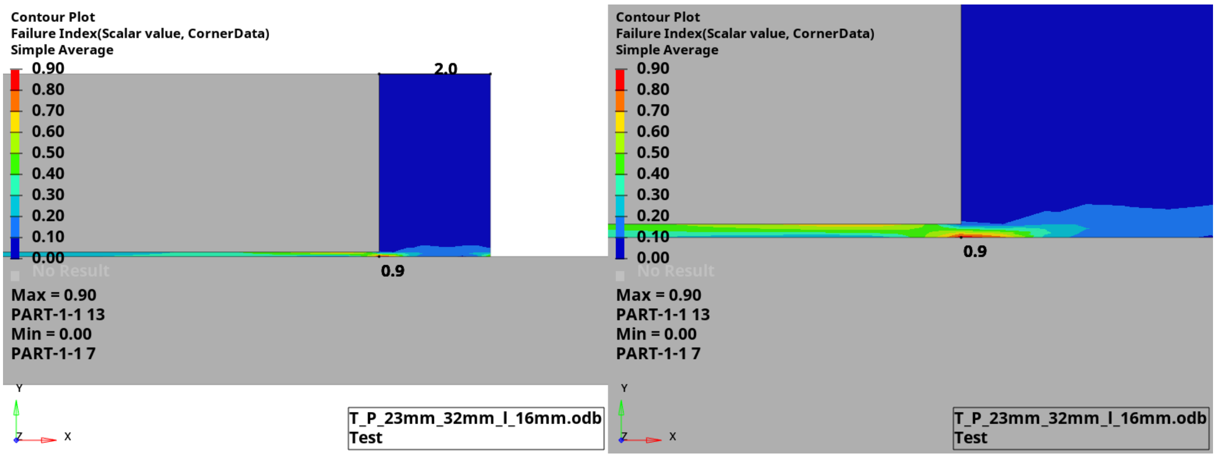

Figure 4.5: Failure index for the SLJ type 6 (left) and its magnified image (right)

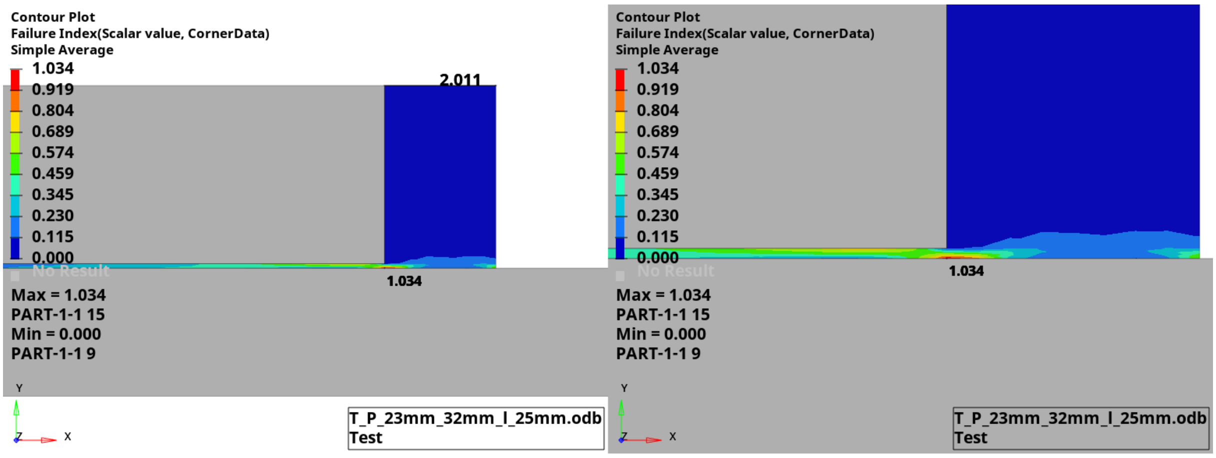

Figure 4.6: Failure index for the SLJ type 8 (left) and its magnified image (right)

4.1.2.2 FE runs

Three FE runs were recreated and their failure indexes are shown in Figures 4.7, 4.8, and 4.9. A conservative equivalent plastic strain based on the failure plastic strain was used in these FE runs. All the three SLJ types have failure index less than 1. Similar to the tested specimens, the failure region or hot-spot is obtained at the interface between adhesive and adherend.

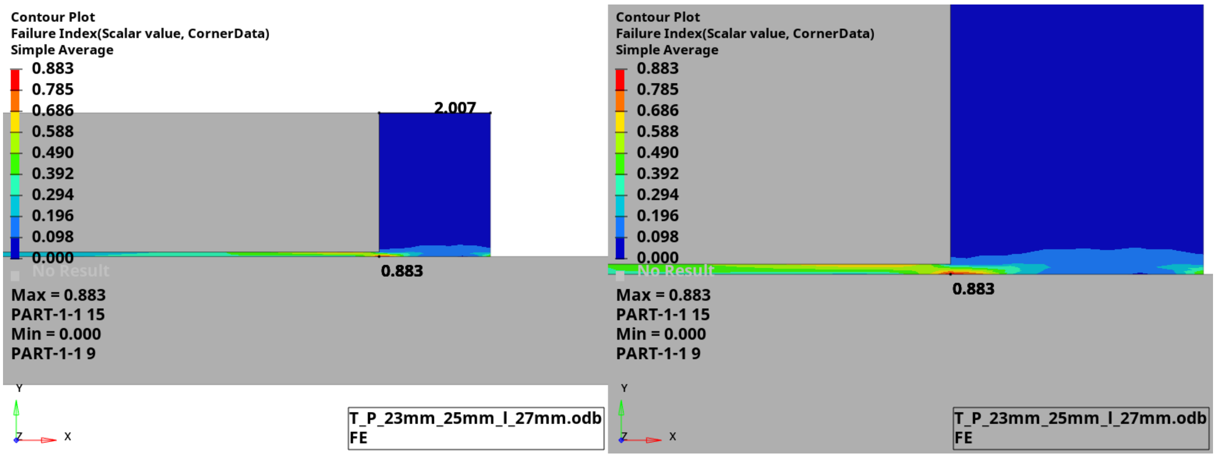

Figure 4.7: Failure index for the SLJ type 5 (left) and its magnified image (right)

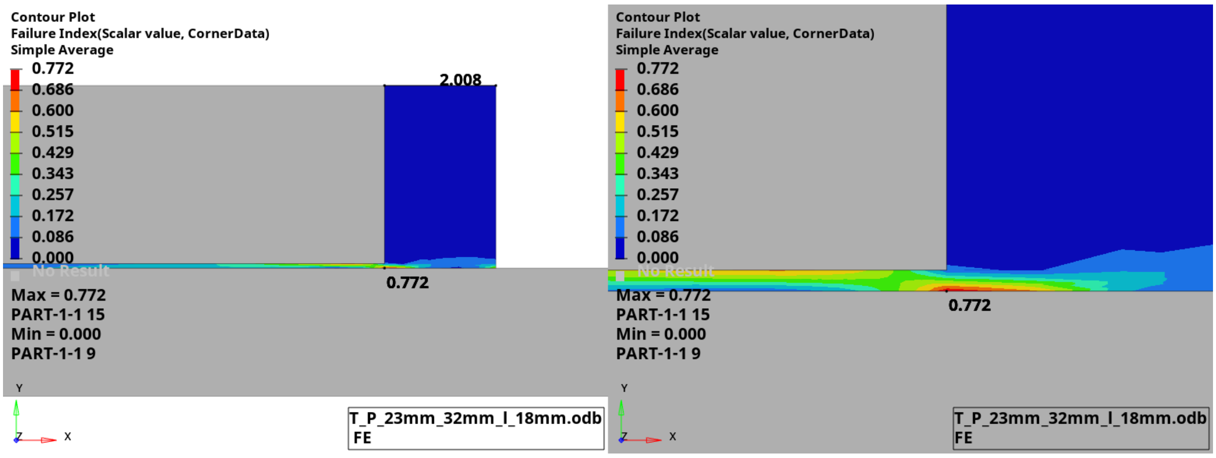

Figure 4.8: Failure index for the SLJ type 7 (left) and its magnified image (right)

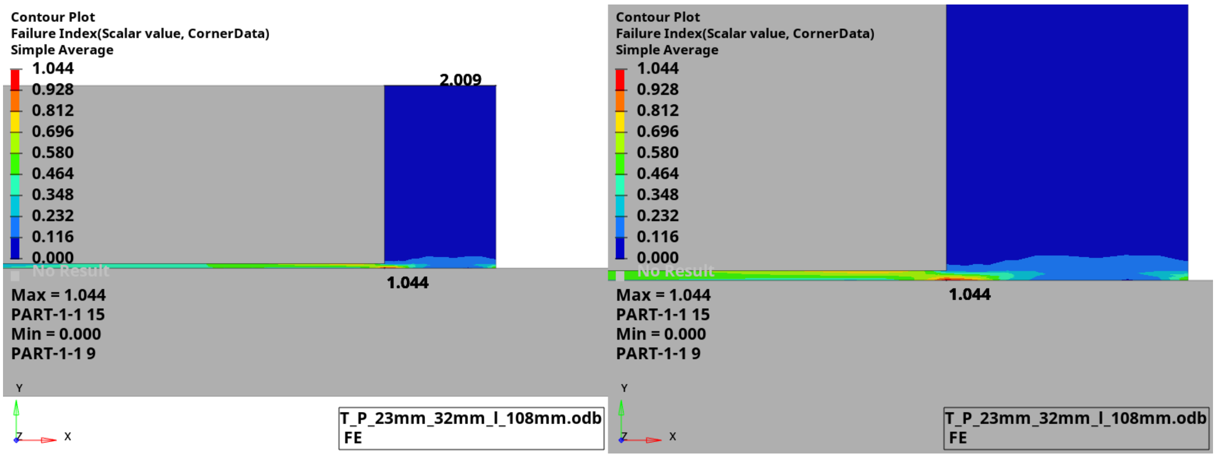

Figure 4.9: Failure index for the SLJ type 9 (left) and its magnified image (right)

4.1.3 Local model 2D to 3D comparison

The adhesive must be modeled with 3D elements in the global model due to the complexity of the loading condition. The purpose of this section is to study the hot-spot region and the magnitude of equivalent plastic strain obtained in comparison of the plane strain (2D) model. The SLJ type 4 is modeled with 3D elements and the results are shown in this section.

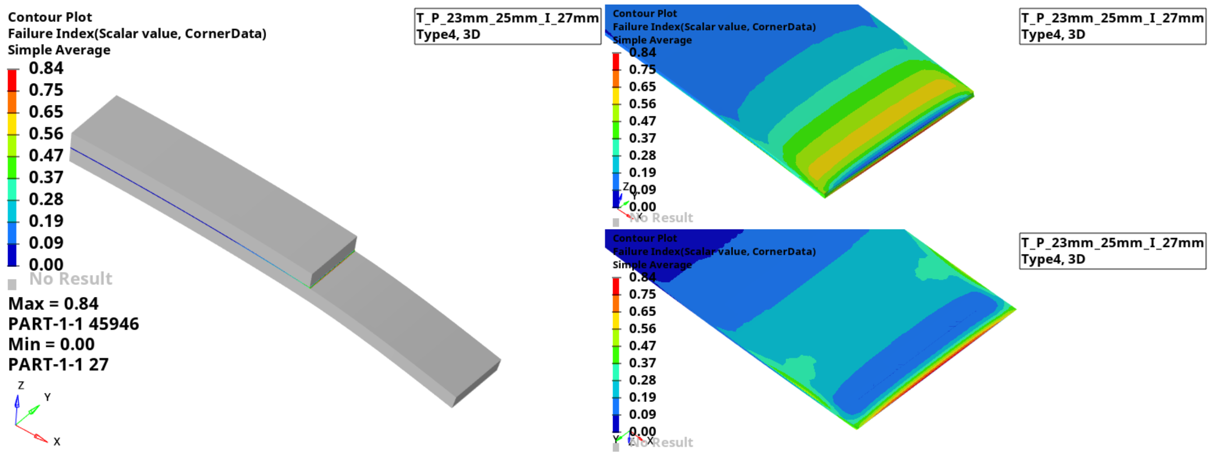

Figure 4.10: Failure index for the SLJ type 4 (left) and a magnified image of the adhesive's top face (top right) and the bottom face (bottom right)

Failure index for SLJ type 4 is shown in Figure 4.10. A failure index of 0.84 is obtained which is less than the plane strain (2D) model as shown in Figure 4.4. The hot-spot is observed at the interface between adhesive and adherend similar to the respective 2D model.

4.1.4 Mesh refinement study for the local model

A mesh convergence study is performed for the local 3D model, and the results are shown in this section. The mesh size is reduced by 50%, and if the result is found to be less than 10%, then the mesh is considered to be converged.

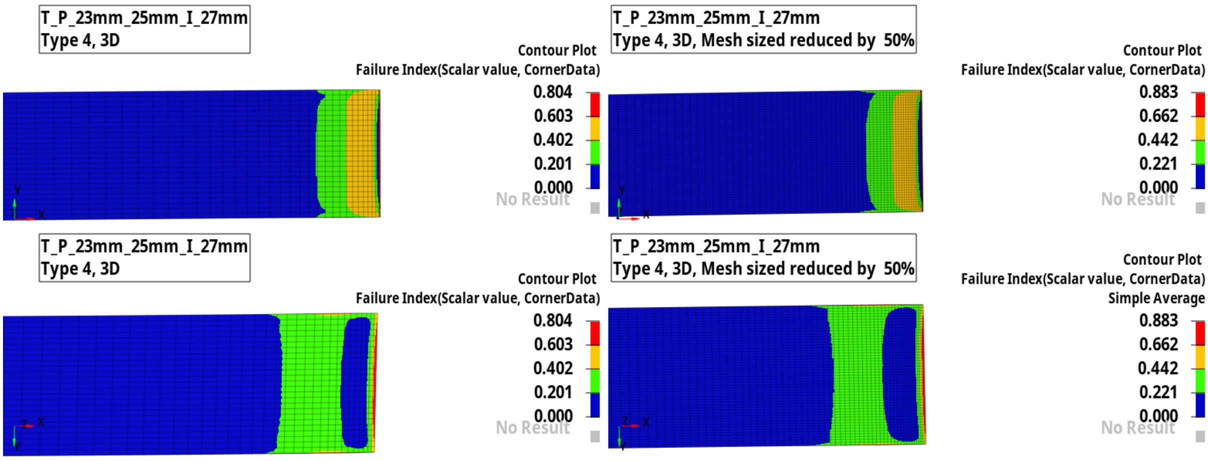

Figure 4.11: Failure index for the original (top and bottom left images) and refined (top and bottom right images) mesh

Figure 4.11 depicts the failure index of the SLJ type 4 for the nominal and the refined mesh. For the nominal model, the failure index is found to be 0.804 while for refined model, it is found as 0.883, which is an increment of 8.9%.

4.2 Global Finite Element Model (GFEM)

4.2.1 Jam load case

Results for the Jam load case are shown in this section.

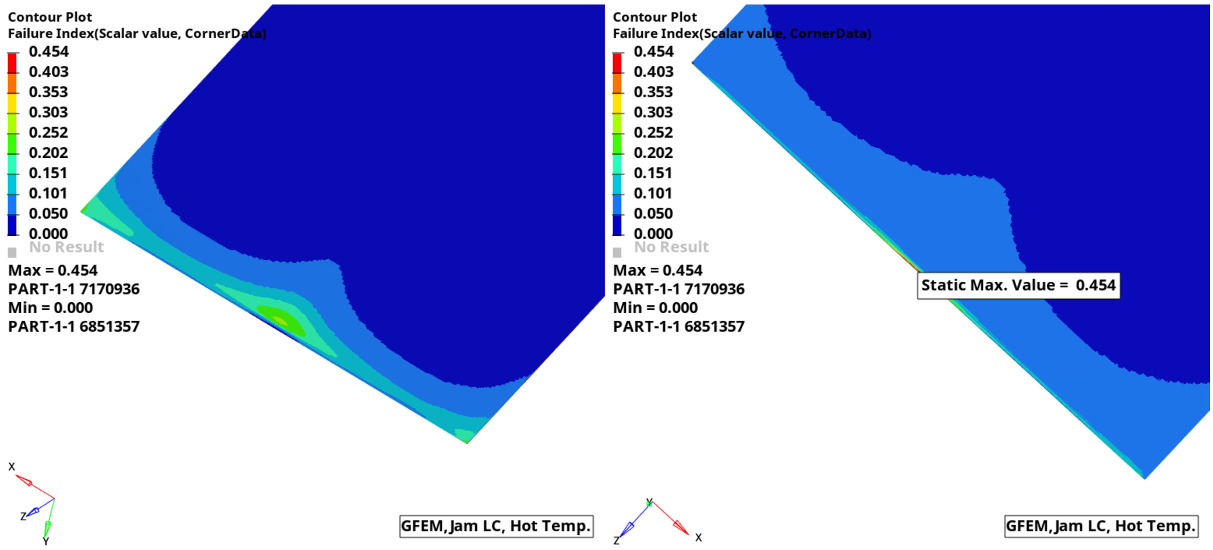

Figure 4.12: GFEM failure index in the adhesive's top (left) and bottom (right) face for Jam load case at the hot temperature

The maximum failure index for Jam load case at hot temperature is obtained as 0.454 as shown in Figure 4.12. The peak stresses can be observed at the centre of the flange. Plasticity is located near the edge of the joint.

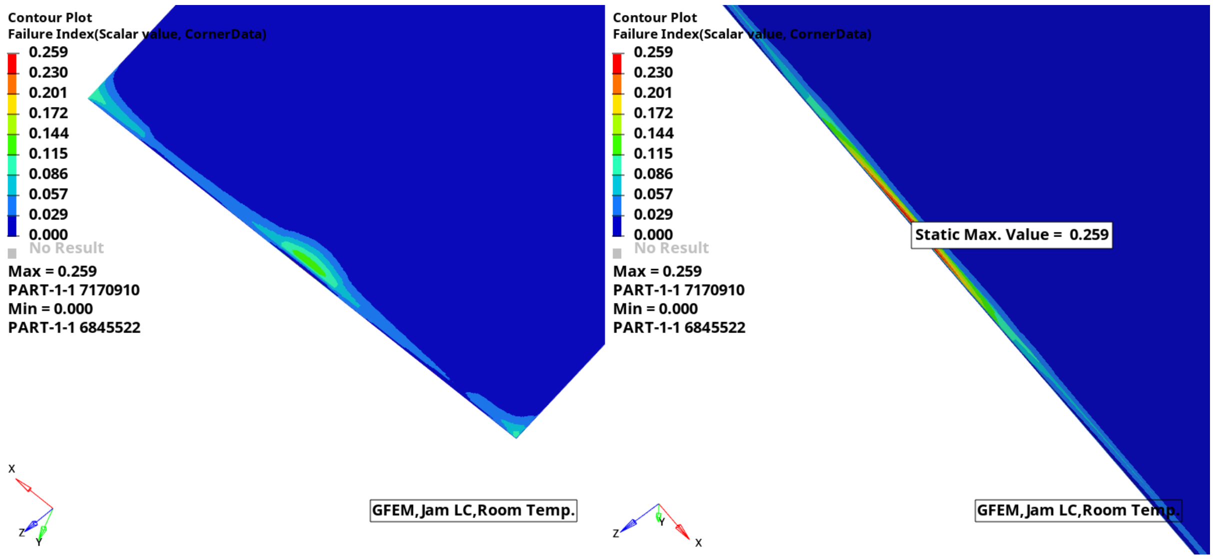

Figure 4.13: GFEM failure index in the adhesive's top (left) and bottom (right) face for Jam load case at the room temperature

A maximum failure index of 0.259 can be observed in Figure 4.13 which is for the Jam load case at room temperature. Similar to the hot temperature load case, plasticity is concentrated at the center of the flange but the plasticized region is less in the room temperature load case.

4.2.2 Ultimate cabin pressurization load case

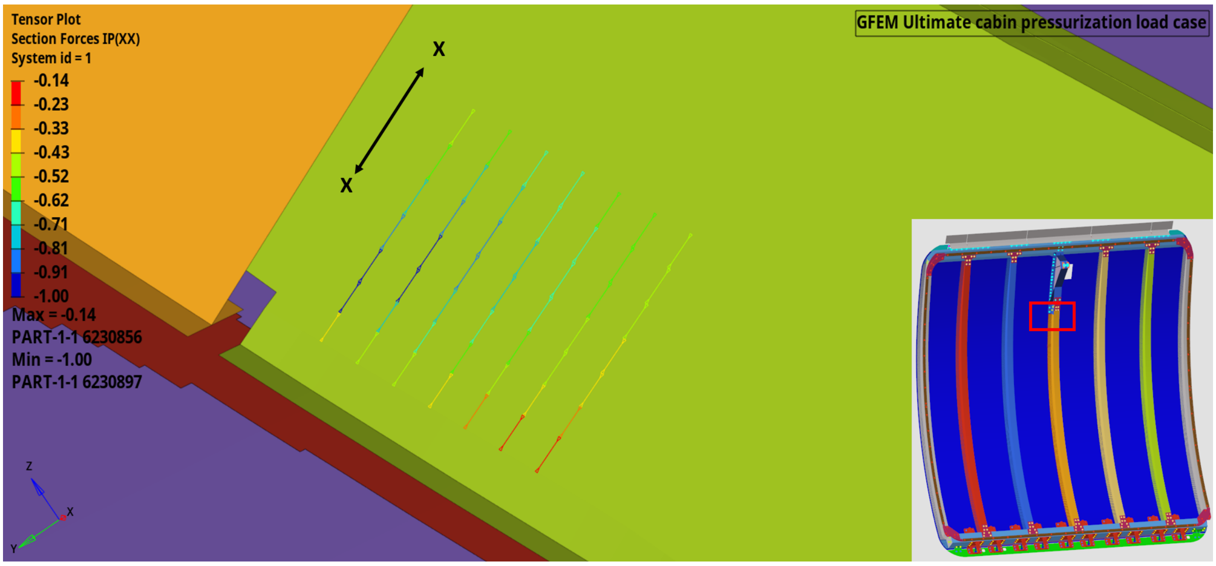

Figure 4.14: Section force at the critical joint in the xx direction

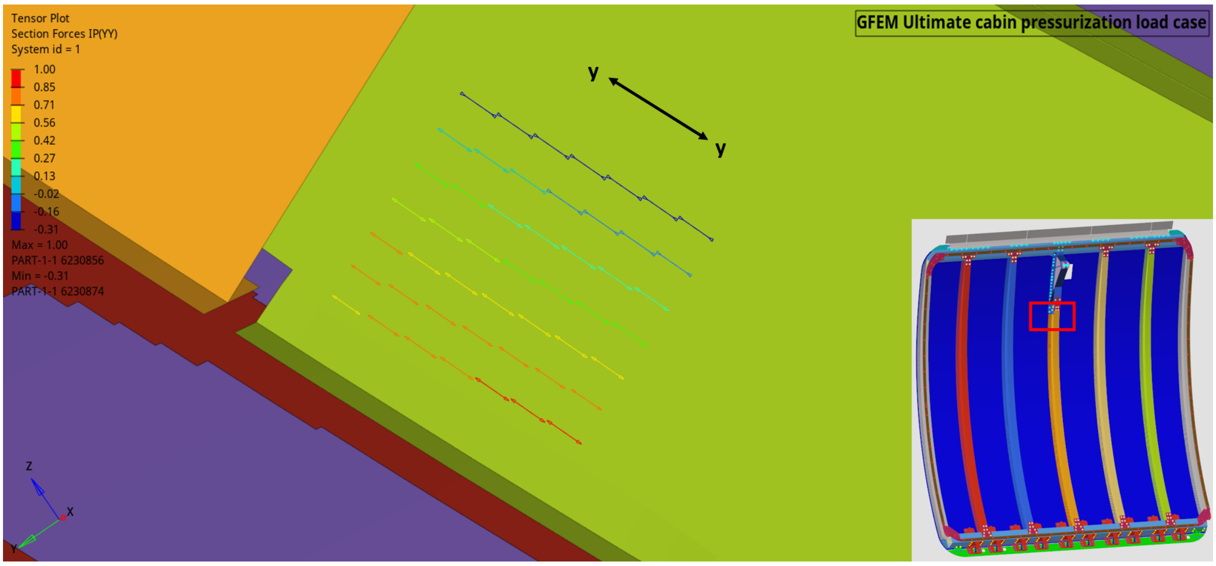

Figure 4.15: Section force at the critical joint in the yy direction

This joint is dominated by tensile loads rather than the peel stresses. The frame web experiences compressive loads in the radial direction (local xx direction) as shown in Figure 4.14, and tensile loads in the hoop direction (local yy direction) as shown in Figure 4.15. Hence, this load case is not critical for the failure due to dominating peel stresses.

5

Proposed test plan

The failure plastic strains for tensile loaded single lap joints are less than the failure plastic strains of transversely loaded joints. Hence, tensile and three-point bending tests are proposed to validate the FE predictions.

5.1 Tensile test

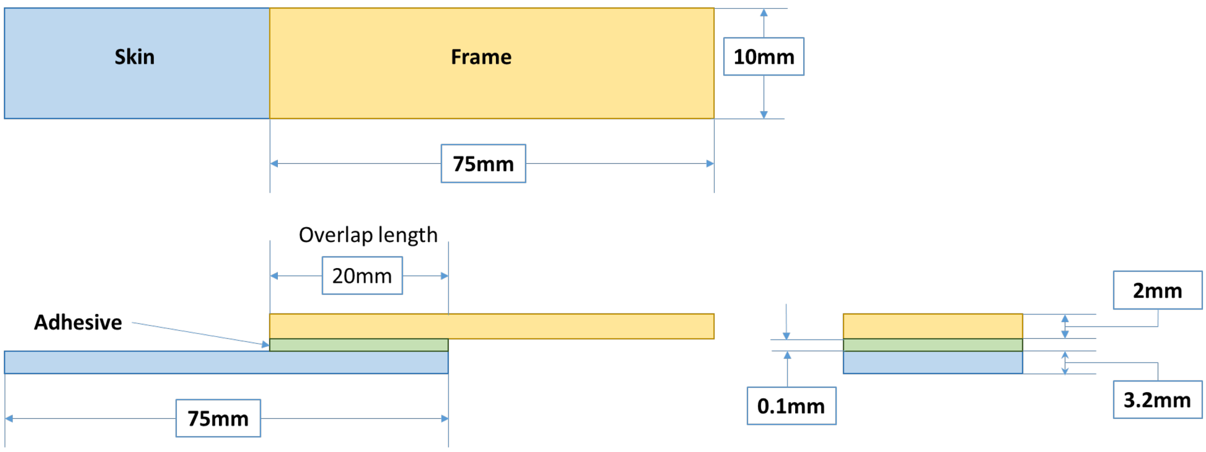

Figure 5.1: SLJ dimension for tensile test

Figure 5.1 shows the test specimen dimensions. The left edge is clamped as shown in Figure 5.2 whereas the right edge is restricted to move in the transverse direction and a longitudinal force of magnitude F is applied. The ultimate cabin pressure is found to be the most critical load case for tensile failure. 292 N/mm is a tensile load intensity per unit width of the frame flange which is obtained by taking average of the all elements in the bottom row shown in Figure 5.3.

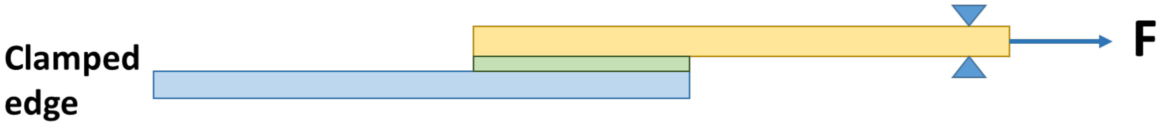

Figure 5.2: Boundary and loading conditions for SLJ tensile test

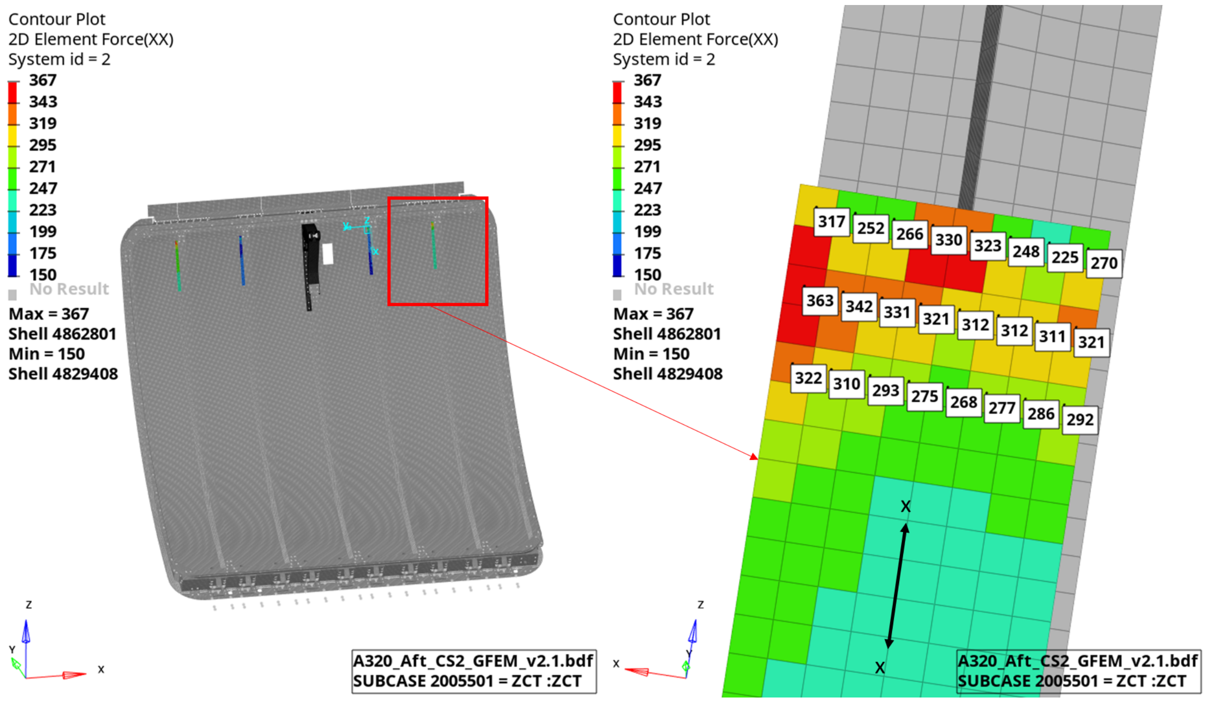

Figure 5.3: The most critical tensile load in GFEM for ultimate cabin pressurization load case

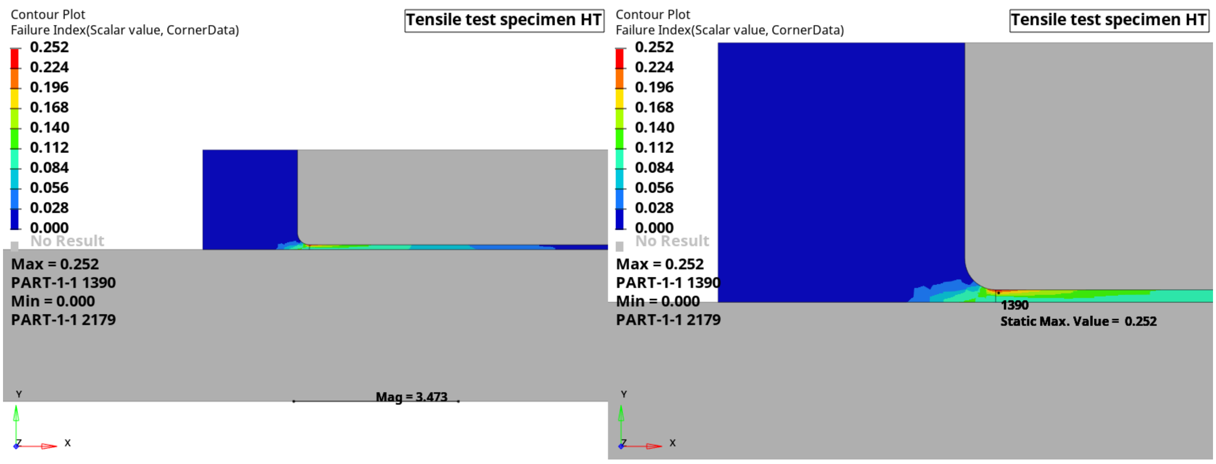

Figure 5.4: Failure index for the tensile test at hot temperature (left) and its magnified image (right)

The tensile test setup is stress analysed and the failure index is shown in Figure 5.4. The plane strain 2D elements have been used along with spew fillets and a fillet of 0.252 mm radius in the adherends. The FE analysis predicts a failure index of 0.252 as shown in Figure 5.4.

5.2 Three point bending test

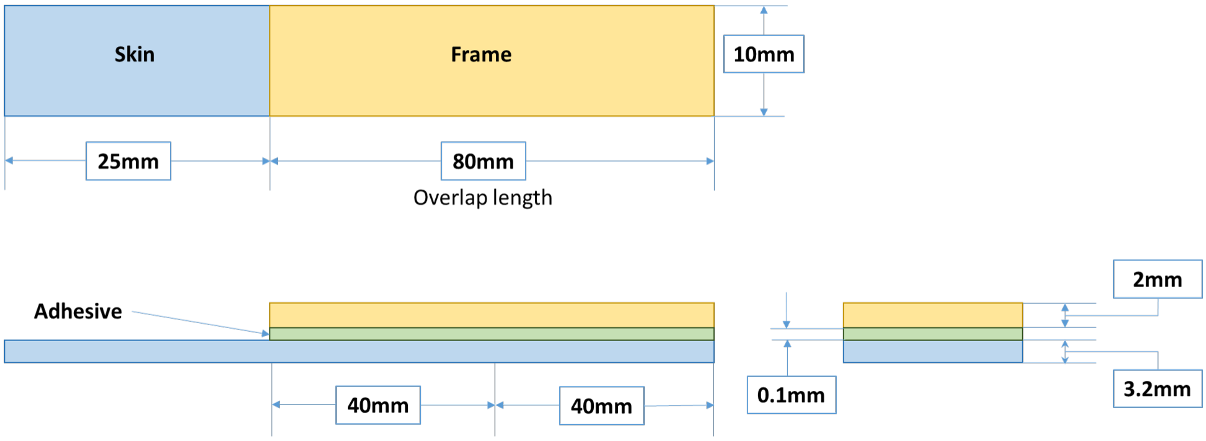

Figure 5.5: SLJ dimension for three point bending test with its top (top left), front (top bottom) and side (bottom right) views

Figure 5.5 shows the test specimen dimensions for three point bending test. This test is designed to capture a peel dominated failure in the SLJ. Loading and boundary condition for this test is shown in Figure 5.6.

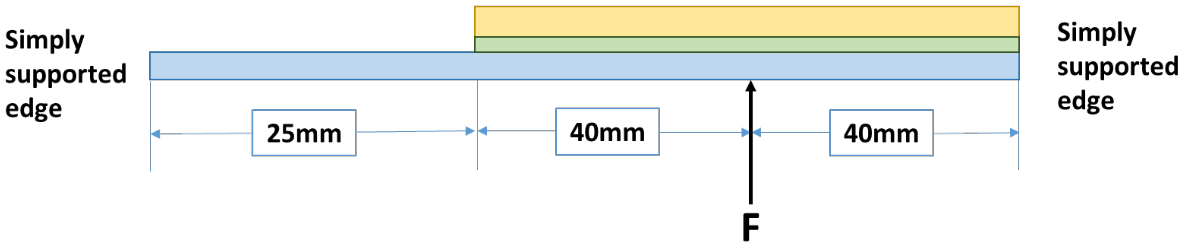

Figure 5.6: Boundary and loading conditions for SLJ three point bending test

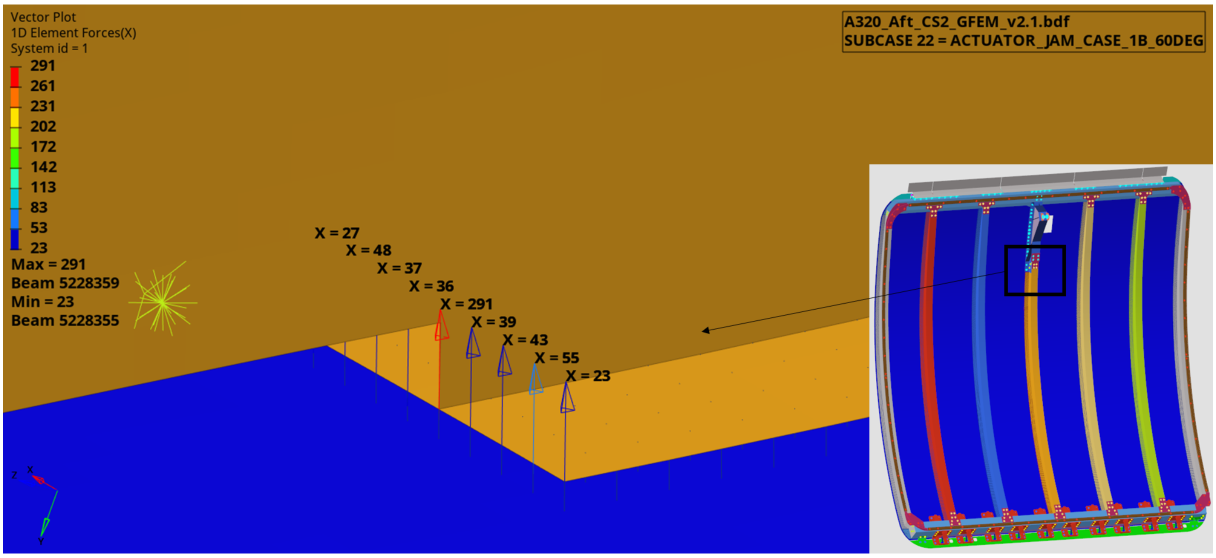

Figure 5.7: The most critical pull load generating peel stress in the adhesive

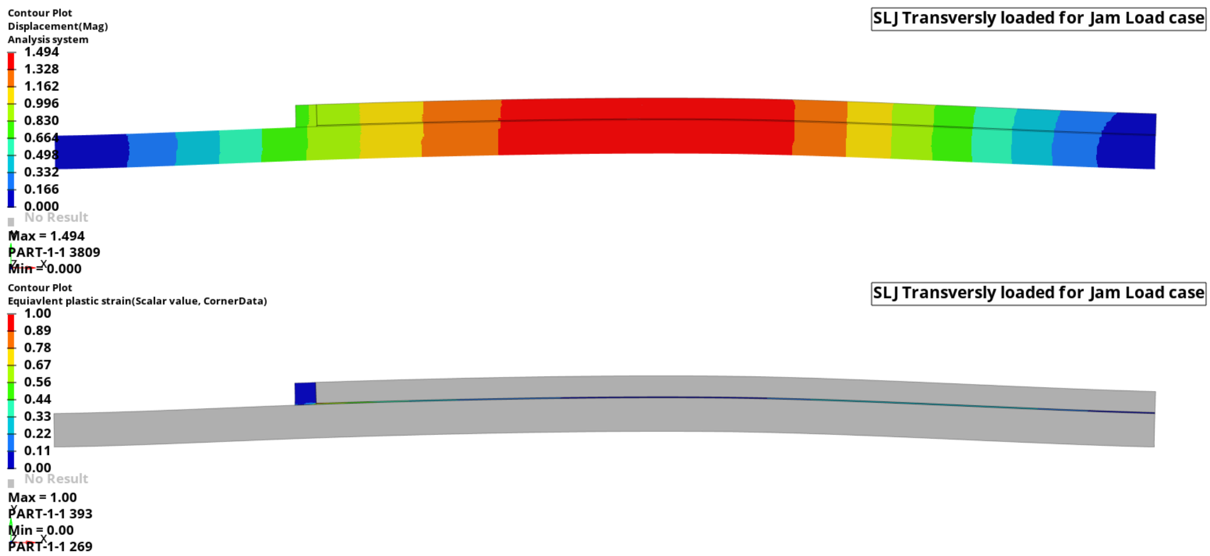

Figure 5.8: Contour plot for displacement (top image) and equivalent plastic strain (bottom image) in the test specimen for Jam load case

The 1D element at the center of the frame flange shown in Figure 5.7 shows higher forces compared to its neighbouring elements. The trial and error method is used to determine the point/line load. The load of magnitude F is manipulated to obtain the equivalent plastic strain (PEEQ [4]) of the Jam load case. Figure 5.8 shows the displacement and equivalent plastic strain plot of the test specimen under an transverse load of 148 N/mm.

6

Conclusions

Adhesively bonded joints under tensile and transverse load are analyzed in this project. Single lap joint with varying geometry are stress analysed. The dimensions of these joints and loads applied are taken from [6] and [7].

The adherends are fabricated from Aluminum and adhesives from AF163-2. The material properties of adhesive FM73M OST are used in the FE models, as the material properties of adhesive AF163-2 is unavailable. The strength predicted in this project is conservative as adhesive AF163-2 shows better strength characteristics than the adhesive FM73M OST.

The stresses and strains of the single lap joint are analyzed by a non-linear FE technique. The plastic material model used for adhesive is the extended Drucker-Prager model and for the adherends it is J2 plasticity (von Mises).

The use of a spew fillet is crucial to reduce the stress singularities in both loading conditions. Along with the spew fillets, the small fillets in the adherend are also used in the SLJs under tensile load to reduce stress singularities. The hot spots in transversely loaded joints are located at the interface between the adherend and the adhesive, while for the tensile loaded joints, they are found near the adherend's fillet at the interface between the adhesive and the adherend.

The local model overestimates the failure of tensile loaded joints which could be the result of incorrect failure strain from the test data. The incorrect adhesive thickness could also lead to faulty results, for instance considering a linear stress response, a thinner adhesive cross-section will experience higher stresses and vice versa.

The used FE technique accurately predicts the failure of transversely loaded joints. The strength prediction based on the extended Drucker-Prager model shows that the load at the critical joint in the cargo door does not reach the failure load while the analytical method in [8] predicts failure. This report also provides a test plan to test the strength of the critical joints in the door. The FE analyses of the most critical joints of the cargo door for the Jam load case and the ultimate cabin pressure case does not predict failure.

Bibliography

[1] J.A. García, A. Chiminelli*, B. García, M. Lizaranzy, M.A. Jiménez. Characterization and material model definition of toughened adhesives for finite element analysis, international Journal of Adhesion & Adhesives 31 (2011) 182-192.

[2] Muhammet Onur Doru, Adnan Özel, Salih Akpinar and Murat Demir Aydin. Effect of the Spew Fillet on Adhesively Bonded Single-Lap Joint Subjected to Tensile Loading: Experimental and 3-D Non-linear Stress Analysis, The Journal of Adhesion, 90:3, 195-209

[3] Jakob, Ring, SAAB AB. Analysis and test definition of adhesively bonded joints in aircraft structures, November 2021

[4] Abaqus Manual

[5] Von Mises yield surface

[6] SAAB internal document for results of tensile test of single lap joint.

[7] SAAB internal document for results of transverse test of single lap joint.

[8] SAAB internal document for static and fatigue justification of the door.

DEPARTMENT OF SOME SUBJECT OR TECHNOLOGY
CHALMERS UNIVERSITY OF TECHNOLOGY
Gothenburg, Sweden
www.chalmers.se

CHALMERS
UNIVERSITY OF TECHNOLOGY